Uniform α-nucleus potential in a wide range of masses and energies

U. Atzrott, P. Mohr, H. Abele, C. Hillenmayer, and G. Staudt
Physikalisches Institut der Universität Tübingen, D-72076 Tübingen, Germany
(Received 11 October 1995)

We have reanalyzed elastic α scattering data on many target nuclei from ^{40}Ca up to ^{208}Pb over a wide range of energies. Using double-folded potentials we have obtained excellent agreement between the experimental scattering data and our optical model calculations. In addition, bound state properties have been calculated successfully. A systematic behavior of the energy and mass dependence of the strengths of the real and imaginary potentials has been found.

PACS number(s): 24.10.Ht, 25.55.Ci

I. INTRODUCTION

Elastic α-nucleus scattering processes are generally described by the optical model employing complex α-nucleus potentials whose parameters are adjusted to reproduce the scattering data. The knowledge of these potentials also plays an important role in the description of many other nuclear reactions, e.g., inelastic scattering processes, transfer or other direct reactions, the calculation of transmission coefficients, and nuclear structure studies. Recently many nuclear processes in astrophysical scenarios have been described by α-nucleus potentials [1–4]. Such processes are radiative capture, transfer reactions, and alpha decay occurring in primordial nucleosynthesis and in stellar hydrostatic and explosive burning modes.

In many investigations complex Woods-Saxon potentials are used. In other analyses the simple Woods-Saxon shape was generalized by introducing terms of higher order of the Woods-Saxon function (e.g., [5,6]). Furthermore, analyses of elastic α-scattering data in terms of model-independent parametrizations of the optical potential have been made using either spline functions (e.g., [5,7]), or a series of Fourier-Bessel functions added to a Woods-Saxon form factor [8,9]. Gubler *et al.* [6] performed a model-independent analysis, expressing the real part of the potential in terms of a sum of Gaussians. Recently, a global optical potential for α particles with energies above 80 MeV using Woods-Saxon-type form factors has been obtained by Nolte *et al.* [10]. It has been extended to lower energies by Avrigeanu *et al.* [11] and proved appropriate to describe (n,α) reactions.

For the real part of the optical potential in the α-^{16}O system Michel *et al.* [5] found a new parametrization. The extracted real potential, which has only two smoothly varying energy-dependent parameters, together with a squared Woods-Saxon form factor for the imaginary potential, gives an exact description of both the α-^{16}O elastic scattering data in the energy range between 30 and 150 MeV and the α-cluster spectroscopy of ^{20}Ne.

A folding approach for α-cluster states in ^{20}Ne and ^{19}F has been presented by Buck *et al.* [12,13]. The α-^{16}O potential was obtained [12] by folding the α cluster and the ^{16}O core using a zero range nucleon-nucleon interaction; for the description of the α cluster states in ^{19}F a potential with a cosh parametrization was used [13], which shape is very similar to the one used in the ^{20}Ne case. In a further work Buck *et al.* [14] have analyzed α-cluster states in ^{20}Ne, ^{44}Ti, ^{94}Mo, and ^{212}Po using a special Saxon-Woods potential with the shape $\alpha \cdot WS + (1-\alpha) \cdot WS^3$. Good agreement with the observables like the energy spectra of the rotational bands, rms radii, $B(E2)$ values, and α-decay widths has been obtained. In these cases the resulting potentials have not been tested versus the elastic scattering data; in two very recent papers Buck *et al.* have shown that their potentials can also be used to calculate elastic scattering cross sections on ^{16}O and ^{40}Ca [15] and ^{208}Pb [16].

Recently, Abele and Staudt [17] have presented a unified description of scattering cross sections as well as bound and quasibound states for the systems $\alpha + ^{16}$O and $\alpha + ^{15}$N. The real part of the potential was calculated using a double folding procedure taken from Ref. [18]. Effective nucleon-nucleon interactions with different density dependencies as well as zero-range and finite-range knock-on exchange terms were investigated. The dispersive part of the real potential was calculated using the dispersion relation of the optical potential. Together with the dominating channel potential it reproduces the observed energy dependence of the volume integral of the real part of the potential. Finally, Abele and Staudt [17] calculated the energies and properties of the bound and resonance α-cluster states in ^{20}Ne and ^{19}F and found good agreement with the experimental data.

Furthermore, our group has measured differential cross sections for elastic and inelastic α scattering on some light nuclei with the mass numbers $19 \leqslant A \leqslant 36$ at incident energies near 50 MeV [19,20]. The analysis of the data using double-folded potentials results in a soft mass dependence of the volume integrals per nucleon pair of the real part of the potential near 50 MeV.

In the present paper we extend our systematic investigation of α-nucleus potentials to intermediate and heavy nuclei with magic proton or neutron numbers. We give the results of potential model calculations using double-folded potentials which describe in a unified way the elastic scattering of α particles on many target nuclei over a wide range of masses and energies, as well as the properties of bound and quasibound α-cluster states for nuclei with $\alpha \otimes$ core structure where the core is a magic or half-magic nucleus.

Together with the results from lighter nuclei [17,19,20]

we present a global and uniform α-nucleus potential over the complete mass region in the energy range from 0 to 150 MeV. Using the double-folded procedure the ambiguity of the phenomenological potentials can be strongly reduced for the description of elastic scattering data. The uniqueness and the energy dependence of the potentials are an important feature with respect to astrophysical applications.

II. THE OPTICAL POTENTIAL

The potential used in the calculations is of the form

$$U_{OM}(r,E)=V_C(r)+V_f(r,E)+iW(r,E), \tag{2.1}$$

where V_C is the Coulomb potential, V_f the real and W the imaginary part of the nuclear potential. The Coulomb term is either taken as the potential of a uniform charged sphere with a radius of r_C = 1.2–1.3 fm or calculated from double folding the experimental charge distributions [21] with the Coulomb interaction $e^2/(\vec{r}_1-\vec{r}_2)$. The difference in the calculated cross sections between both methods is negligible in this work.

The real part V_f is described in the framework of the double folding (DF) model of Kobos *et al.* [18] by

$$V_f(r,E)=\lambda\int\int d\vec{r}_1 d\vec{r}_2 \rho_T(\vec{r}_1)\rho_\alpha(\vec{r}_2) \times t(E,\rho_T,\rho_\alpha,\ \vec{s}=\vec{r}-\vec{r}_1+\vec{r}_2), \tag{2.2}$$

where $\vec{r}$ is the separation of the center of mass of the target and the projectile, ρ_T and ρ_α are the respective nucleon densities, $t(E,\rho_\alpha,\rho_T,\vec{s})$ is the nucleon-nucleon interaction (NNI), and λ is a potential strength parameter in the range around 1.3.

In coincidence with our results about the influence of different NNI and the effects of zero-range versus finite-range exchange terms to the quality of the fits [17] we use for the NNI the numerical convenient form of [18]. In detail this means

$$t(E,\rho_1,\rho_2,\vec{s})=g(E,|\vec{s}|)\cdot f(E,\rho_T,\rho_\alpha), \tag{2.3}$$

with

$$g(E,s:=|\vec{s}|)=7999\frac{e^{-4.0s}}{4.0s}-2134\frac{e^{-2.5s}}{2.5s}+J_{00}(E_{\text{c.m.}})\,\delta(s), \tag{2.4}$$

$$J_{00}=-276\left(1-0.005\frac{E_{\text{c.m.}}}{\mu}\right), \tag{2.5}$$

$$f(E,\rho_1,\rho_2)=C(E)[1+\alpha(E)e^{-\beta(E)(\rho_1+\rho_2)}], \tag{2.6}$$

where $E_{\text{c.m.}}$ is the center-of-mass energy of the experiment in MeV, μ is the reduced mass number of the α-core system, and C,α, and β are obtained through fitting the volume integral of $t(E,\rho_1,\rho_2,\vec{s})$ to the strength of the real part of a G-matrix effective interaction obtained from Brueckner-Hartree-Fock calculations [22,23]. C,α, and β have been calculated using the code WWFIT [24].

The nucleon densities in Eq. (2.2) are derived from experimental charge distributions [21] by unfolding the finite charge distributions of neutron and proton [25]. The assumption $\rho_{\text{proton}}=(Z/N)\rho_{\text{neutron}}$ was used except for ^{208}Pb, where a theoretical neutron distribution [26] was added to the proton mass distribution derived from the experimental charge distribution. The experimental charge distribution of the α particle was taken as a sum-of-Gaussian [21]. For the imaginary part different parametrizations such as, i.e., Woods-Saxon functions or Fourier-Bessel series were employed.

To compare our folding potentials to potentials with different parametrizations we calculated the volume integrals J and the root-mean-square radii r_{rms} which are given by

$$J_R(E)=\frac{4\pi}{A_T A_\alpha}\int_0^\infty V_f(r,E)r^2dr \tag{2.7}$$

and

$$r_{\text{rms},R}=\langle r^2\rangle^{1/2}=\left(\frac{\int V_f(r,E)r^4dr}{\int V_f(r,E)r^2dr}\right)^{1/2} \tag{2.8}$$

for the real part and corresponding definitions for the imaginary part.

According to the causality principle there has to be a relation between the real and the imaginary part of the potential because scattering cannot occur before the interaction. Mahaux, Ngo, and Satchler [27] and Pacheco *et al.* [28] gave a dispersion relation for the equivalent local potential which has been proved in a recent work of Pantis *et al.* [29],

$$\Delta V(r,E)=\frac{1}{\pi}\mathscr{P}\int_{-\infty}^{+\infty}\frac{W(r,E')}{E'-E}dE', \tag{2.9}$$

with $\mathscr{P}$ denoting the Cauchy principal value. The dispersion relation (2.9) also holds for volume integrals

$$\Delta J_R(E)=\frac{1}{\pi}\mathscr{P}\int_0^{+\infty}\frac{J_I(E')}{E'-E}dE'. \tag{2.10}$$

In order to avoid difficulties resulting from the normalization of the integral in Eq. (2.10) one usually uses the subtracted dispersion relation

$$\Delta J_R(E)-\Delta J_R(E_S) =(E-E_S)\frac{1}{\pi}\mathscr{P}\int_0^{+\infty}\frac{J_I(E')}{(E'-E_S)(E'-E)}dE', \tag{2.11}$$

where E_S is a reference energy in the region of interest. Because the knowledge about the behavior of the imaginary part of the potential is small for energies above 200 MeV one should use a reference energy between 30 and 150 MeV.

The volume integral J_I of the imaginary potential can be parametrized by

$$J_I(E)=\begin{cases} E<E_0 & : \quad 0, \\ E\geq E_0 & : \quad J_0\dfrac{(E-E_0)^2}{(E-E_0)^2+\Delta^2}, \end{cases} \tag{2.12}$$

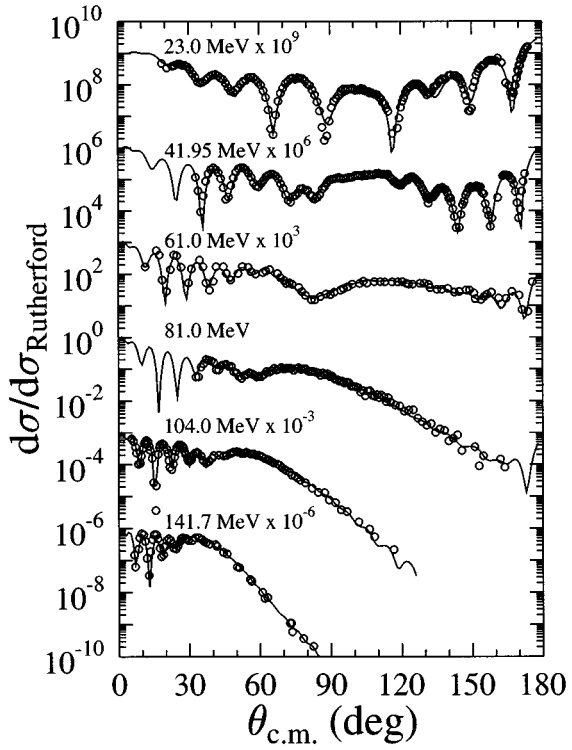

FIG. 1. Elastic α scattering on ^{40}Ca: Experimental data and OM calculations using double-folding potentials, at incident energies of 23, 41.95, 61, 81 MeV [36], 104 MeV [38], and 141.7 MeV [37].

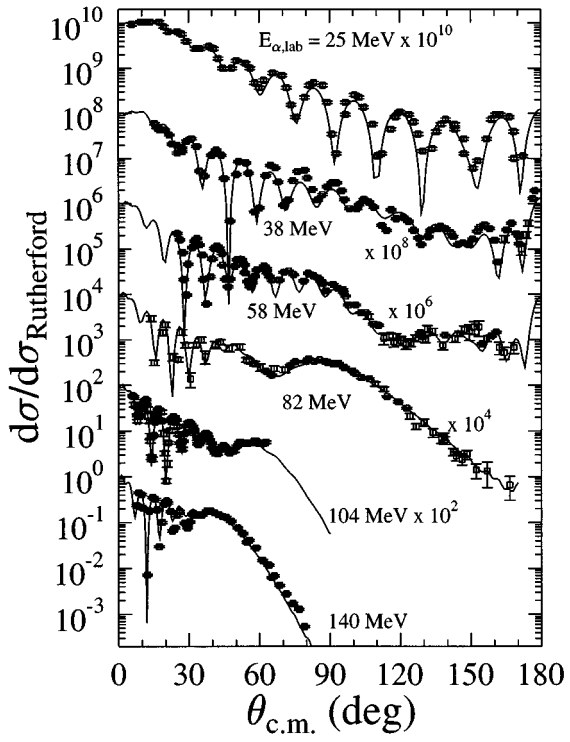

FIG. 2. Elastic α scattering on ^{58}Ni: Experimental data and OM calculations using double-folding potentials, at incident energies of 25 MeV [39], 38 and 58 MeV [40], 82 MeV [42], 104 MeV [43], and 140 MeV [44].

following Brown and Rho [30] (BR parametrization) where E_0 is the threshold energy for inelastic channels, Δ and J_0 are fitting parameters. The integral in Eq. (2.9) can be calculated only under certain assumptions for the high energy behavior of J_I. Mahaux *et al.* [27] and our group [17] showed that the values of J_I for high energies affect only the normalization of J_R. This uncertainty is avoided in using the subtracted dispersion relation (2.11). Different parametrizations assuring the convergence of Eq. (2.9) for the high energy behavior of J_I have been tested; the difference in ΔJ_R is negligible. Therefore we use a linear decrease of J_I in the range 250 MeV $<E<E_L$ with $E_L=10^{20}$ MeV and $J_I(E_L)=0$ MeV.

In order to test the radial dependence of the DF potentials a model independent analysis (MIA) has been applied to specific α-nucleus systems where numerical scattering data of high accuracy and very good statistics covering a large range of momentum transfer were available. Following Andresen and Müller [31] and Clement *et al.* [32] the potential was expanded in a Laguerre series

$$V_{\mathrm{MIA}}(r)=U_{\mathrm{OM}}(r)+\Delta V_{\mathrm{MIA},R}(r)+i\Delta V_{\mathrm{MIA},I}(r) \tag{2.13}$$

with U_{OM} being the best-fit optical model (OM) potential,

$$\Delta V_{\mathrm{MIA},R/I}(r)=\sum_{i=1}^{n_{R/I}} c_{i_{R/I}} e^{-X^2} L_i^{1/2}(2X^2), \tag{2.14}$$

$X=r/a_{R/I}$, $a_{R/I}$ being a scaling parameter, and $L_i^{1/2}$ being the generalized Laguerre polynomials. The coefficients $c_{i_{R/I}}$ and the parameters $a_{R/I}$ and $n_{R/I}$ have been varied until a minimum in χ^2/N has been reached, $N=Z-n_R-n_I$ being the number of degrees of freedom and Z being the number of data points. Then one can calculate error bands following the formulas given by Friedman and Batty [8] and Ermer [33].

The corrections ΔV_{MIA} arising from the Laguerre series in Eq. (2.13) [respectively Eq. (2.14)] to the best-fit OM potential U_{OM} are small.

III. DIFFERENTIAL CROSS SECTIONS

A. Analyses with DF potentials

We have reanalyzed the elastic α-nucleus scattering over a wide range of energies in the mass region between $40 \leqslant A \leqslant 208$. The calculations were done using the codes GOMPF [34] and ECIS79 [35], which have been tested to give the same results.

We consider the scattering on ^{40}Ca in the optical model at 14 energies in the energy range from 23 up to 166 MeV [36–38]. In the α-^{58}Ni system we have reanalyzed the data at 15 energies between 25 and 340 MeV [39–47], and in the α-^{60}Ni system at 10 energies between 15 and 340 MeV [39–41,43,45,48]. For the α-^{90}Zr system a large number of elastic scattering data has been published. We considered the experimental results at 12 energies in the range from 15 to 166 MeV [7,49–55]. The elastic α scattering on nuclei with 82 neutrons has not been covered as extensively as the scattering on other magic nuclei. Most of the data are at relatively small energies ($E<$ 50 MeV) [56,57] with the exception of the 120 MeV data of Ichihara *et al.* [58] on ^{144}Sm. In the α-^{208}Pb system we have analyzed data at 13 energies in

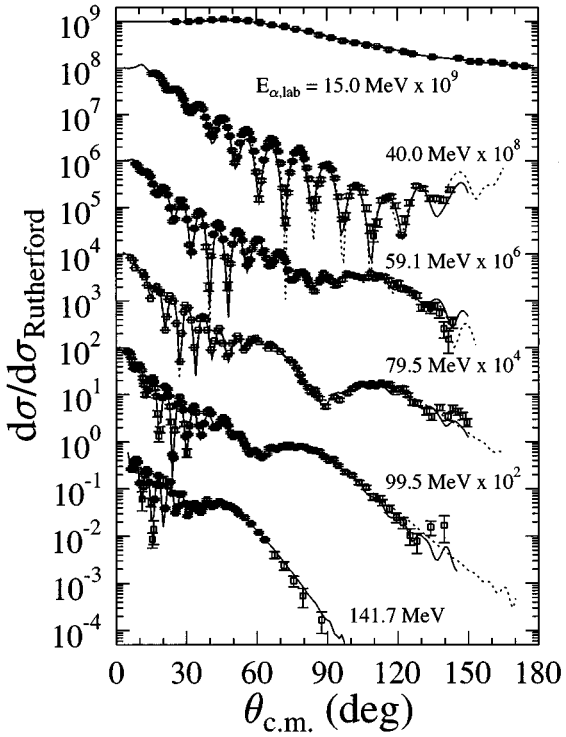

FIG. 3. Elastic α scattering on ^{90}Zr: Experimental data, OM calculations using double-folding potentials (solid lines) and Laguerre series (dotted line), at incident energies of 15 MeV [49], 40, 59.1, 79.5, and 99.5 MeV [7], and 141.7 MeV [54].

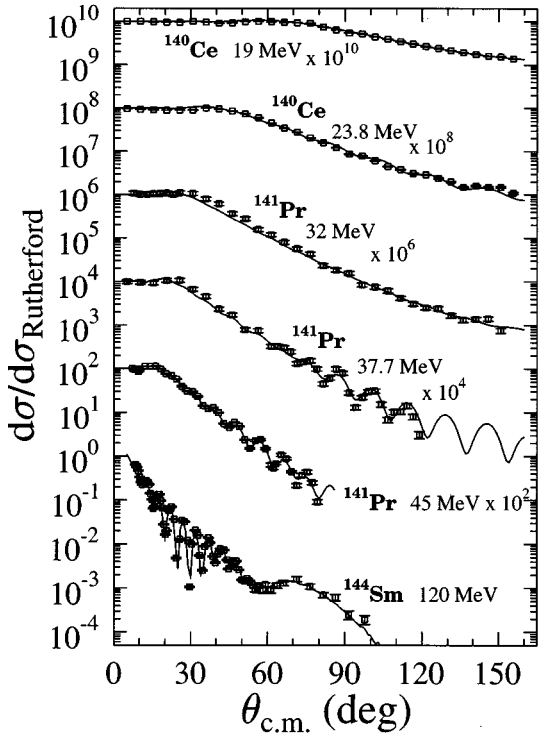

FIG. 4. Comparison between experimental data and OM calculations for elastic α scattering for nuclei with $N=82$: ^{140}Ce (19 and 23.8 MeV) [56], ^{141}Pr (32 and 37.7 MeV) [56] and 45 MeV [57], and ^{144}Sm (120 MeV) [58].

the range between 23.5 and 340 MeV [46,47,59–66].

The charge distributions used for calculating the real part of the nuclear potential by a double folding procedure were taken from de Vries *et al.* [21] (sum-of-Gaussian for ^{40}Ca, ^{58}Ni, and ^{208}Pb, Fourier-Bessel for ^{60}Ni and ^{144}Sm, 3-parameter-Gaussian for ^{90}Zr, and 2-parameter-Fermi-distributions for ^{140}Ce, and ^{141}Pr).

The Coulomb part of the α-nucleus potential was calculated either by double folding the experimental charge distributions with the Coulomb interaction (^{40}Ca and ^{208}Pb) or from the field of a uniform charged sphere with radius parameters of $r_C = 1.2$ fm (Ni), $r_C = 1.25$ fm (Zr), and $r_C = 1.3$ fm ($N=82$).

For the imaginary part of the potential different parametrizations were chosen. In the case of ^{40}Ca it is described by a Fourier-Bessel series: $W(r)=\Sigma_{k=1}^{8} a_k \cdot j_0(k\pi r/R_{cut})$. The cutoff radius parameter was chosen as $R_{cut} = 10$ fm for energies below 100 MeV and $R_{cut} = 12$ fm otherwise. For the Ni isotopes a sum of a squared Woods-Saxon (WS) volume term and a surface term was applied. For ^{90}Zr and $N=82$ nuclei a volume WS was added to a surface WS potential. In the case of ^{208}Pb a squared WS potential proved to be sufficient.

In order to minimize the number of figures and tables we show only some results for the differential cross sections in Figs. 2–7. The complete results of our analysis are available from the authors. The integral values of the potentials used for the calculations are listed in Table I for some of the energies analyzed.

As can be seen from the figures, in all cases a good agreement between the experimental data and the results of the calculations is obtained.

For α-^{40}Ca the integral values of the potential agree well with the results of Delbar *et al.* [37], who have analyzed their data using $(WS)^2$ potentials, and with the results of Gubler *et al.* [6] where a sum-of-Gaussian was used to calculate the potentials.

For the target nuclei ^{58}Ni and ^{60}Ni the quality of the description of the angular distributions is more or less identical; therefore no figures are shown for ^{60}Ni. Also the differences in the volume integrals are negligible. The values obtained agree with the results given by Budzanowski *et al.* [40] who used potentials with $(WS)^2$ form factors in their analysis. Friedman *et al.* [67] report $J_R=287$ MeV fm^3 and $J_I=93$ MeV fm^3, extracted from a model independent analysis at 140 MeV, compared with 278 MeV fm^3 and 98 MeV fm^3, respectively, found in this work. Good agreement is also found with the results of Khoa *et al.* [68] who analyzed data at 139 and 172.5 MeV in the frame of a double-folding model with full finite-range effective NN interaction.

For α-^{90}Zr we find good agreement with the results of Kobos *et al.* [18] who have analyzed the data for the first time with a double-folded potential using the density dependent form of the M3Y effective NNI. The analyses of Put and Paans [7] by fitting the ^{90}Zr data using six-parameter WS potentials result in values for the volume integrals for the real part of the nuclear potential which are about 10–20 %

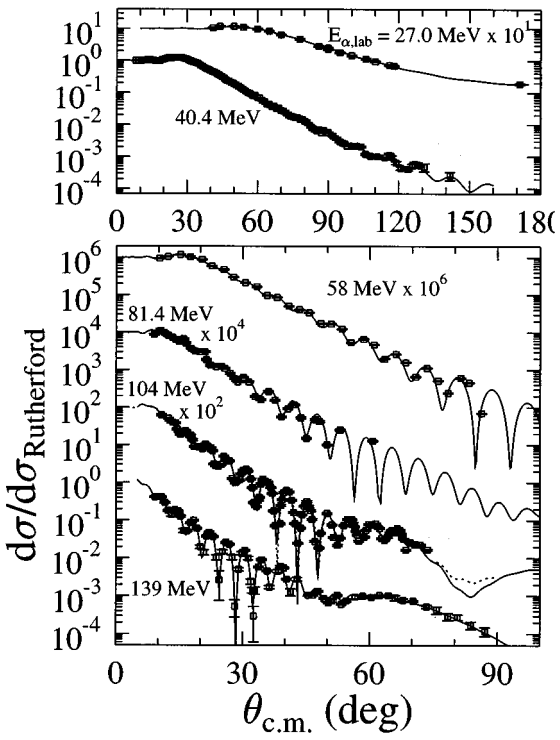

FIG. 5. Elastic α scattering on ^{208}Pb: Experimental data and OM calculations using double-folding potentials, at incident energies of 27.0 MeV [59], 40.4 MeV [61], 58 MeV [63], 81.4 MeV [64], 104 MeV [65], and 139 MeV [66]. The dashed line (104 MeV data) is the result of a model independent analysis.

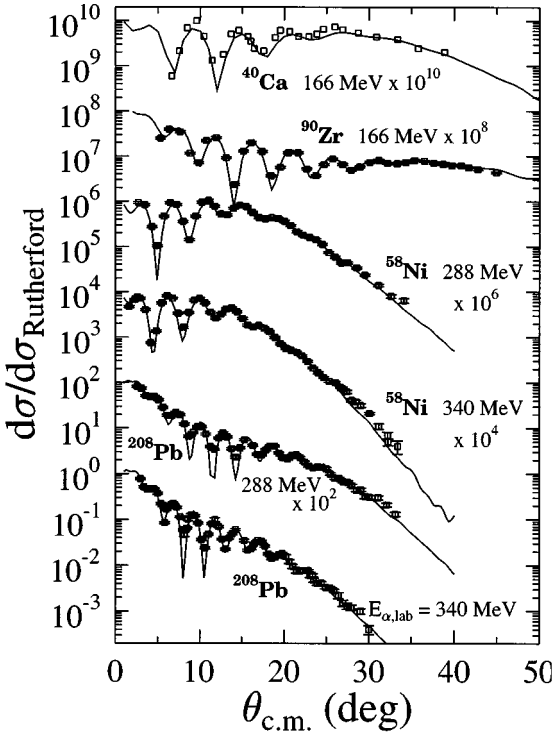

FIG. 6. Comparison between experimental data and OM calculations for elastic α scattering for energies above 160 MeV: ^{40}Ca (166 MeV) [37], ^{90}Zr (166 MeV) [55], ^{58}Ni (288 and 340 MeV) [47], and ^{208}Pb (288 and 340 MeV) [47].

higher than our values whereas those for the imaginary part are similar. Friedman *et al.* [67] report J_R = 289 MeV fm^3 and J_I=84 MeV fm^3 at E_α=140 MeV compared with 273 MeV fm^3 and 82 MeV fm^3, respectively, found in our analyses. In contradiction to their earlier results on the α-^{58}Ni scattering and to our results on α-^{16}O scattering Khoa *et al.* [68] find a notable difference in the analysis of the α-^{90}Zr data if the potential is calculated in finite-range (FR) or zero-range exchange (ZR). Their integral values calculated in ZR are considerably higher than those calculated in FR approximation. A further consideration of NN correlations leads to values for J_R that are consistent with our results. Recently, Ohkubo [69] has calculated the elastic α scattering on ^{90}Zr in the energy range from 23 to 80 MeV. For his calculations he applied the same double-folding model as has been used in this work. He found an increasing potential strength parameter λ with increasing energy. The same behavior has been found in this work over a wider range of energies. But together with the decreasing strength of the NNI one obtains the energy dependence of the volume integrals of the real potential which is shown in Fig. 10. (Small differences in the parameter λ between Ref. [69] and this work may come from the use of different Coulomb radii and/or different parametrizations of the densities of α or ^{90}Zr.) The volume integrals J_R which are more important than the strength parameters λ should agree quite well in both analyses. Unfortunately, these numbers are not given in Ref. [69].

For the N=82 isotopes analyzed in the present work, the volume integrals of the real part of the nuclear potential J_R lie around 335 MeV fm^3 for low energies and around 285 MeV fm^3 for 120 MeV. This is in good agreement with the ^{90}Zr and the ^{208}Pb values. Ichihara *et al.* [58] have performed a detailed OM analysis of their α-^{144}Sm scattering data at 120 MeV, looking for potential differences resulting from different mass distributions. They give a squared WS form factor which lies well within the error band resulting from their model independent analyses using a Fourier-Bessel series. The DF potential obtained in the present work is in very good agreement with the WS^2 potential of Ref. [58] as well in the volume integral (J_R=286.8 MeV fm^3 versus J_R=291.3 MeV fm^3) as in the radial dependence, where the two potentials show almost no difference for radii greater than 3 fm and only small differences for smaller radii.

In the case of the α-^{208}Pb scattering our volume integrals J_R are comparable to those of Perry *et al.* [64] and those of Goldberg *et al.* [66]. The comparison with papers devoted to the ''family problem'' reveals that the DF potentials obtained correspond with those potential families used in the analyses of Refs. [64,66] which result in the smallest volume integrals. Our values for J_R at E_α = 104 MeV are in good agreement with the results of Corcialciuc *et al.* [65] and with the ones obtained by fitting the differential cross sections at E_α = 23.5, 79.1, 104, and 139 MeV under consideration of the coupling to the 3_1^- (2.615 MeV) state [70].

TABLE I. Normalization parameters, volume integrals, and rms radii of the OM potentials for energies around 30, 60, 100, and 140 MeV for the elastic α scattering on ^{40}Ca, ^{58}Ni, ^{60}Ni, ^{90}Zr, $N=82$ nuclei, and ^{208}Pb. In addition the references of the experimental data are given.

	$E_{\rm lab}$ MeV	λ	J_R MeV fm^3	$r_{{\rm rms},R}$ fm	J_I MeV fm^3	$r_{{\rm rms},I}$ fm	Ref.
^{40}Ca	29.1	1.326	362.81	4.272	33.40	3.991	[36]
	61.0	1.300	341.84	4.277	85.10	4.898	[37]
	104.0	1.239	302.50	4.288	101.91	4.908	[38]
	141.7	1.241	281.15	4.303	110.59	4.994	[37]
^{58}Ni	29.0	1.310	350.17	4.531	89.11	4.269	[40]
	59.6	1.308	331.66	4.537	84.57	5.204	[41]
	104.0	1.294	300.82	4.551	93.63	5.288	[43]
	140.0	1.300	278.14	4.570	98.17	5.106	[44]
^{60}Ni	29.0	1.320	350.08	4.542	90.06	4.329	[40]
	60.0	1.266	319.32	4.547	93.97	5.089	[41]
	104.0	1.298	298.02	4.562	92.99	5.359	[43]
^{90}Zr	31.0	1.286	334.54	4.974	77.37	5.294	[51]
	59.1	1.297	314.79	4.979	80.22	5.796	[7]
	104.0	1.279	290.01	4.993	82.50	5.913	[53]
	141.7	1.318	273.29	5.014	81.53	5.911	[54]
^{140}Ce	32.0	1.340	338.55	5.492	83.13	7.825	[56]
^{141}Pr	45.0	1.328	334.51	5.585	61.35	6.728	[57]
^{144}Sm	120.0	1.333	286.89	5.600	79.02	6.80	[58]
^{208}Pb	27.0	1.308	341.81	6.268	40.43	7.520	[60]
	61.5	1.303	322.42	6.272	66.81	7.225	[64]
	104.0	1.310	298.26	6.282	71.30	7.383	[65]
	139.0	1.375	289.48	6.298	75.62	7.262	[66]

B. Model independent analysis

In order to test the radial form of the double-folding potentials used in our analyses we have performed some model independent analyses (MIA). We have applied this method to the ^{90}Zr data of Put and Paans [7] and the 104 MeV data on ^{208}Pb of Corcialciuc *et al.* [65].

The data of Put and Paans have been chosen for two reasons: first of all, the data cover a large range of momentum transfer and are of high accuracy; and second, the data were available in numerical tables. This is important because the experimental uncertainties dominate the shape of the error band. A Laguerre series was applied for the potential. The MIA calculations have been performed using a modified version of the code ECIS90 [71], the error bands have been calculated using the code READECIS [72].

For two energies the radial behavior of the potentials extracted by the MIA is shown in Fig. 1. The differential cross sections, calculated with the MIA potential, are drawn in Fig. 4 as dotted lines. The differences in the description of the experimental data between the DF and the MIA potential are small. For all energies analyzed the DF potentials lie within the 1σ error band of the MIA. The potentials are well determined for radii >4 fm, whereas the error bands tend to grow in the nuclear interior. The imaginary potentials are well determined for large radii ($r>8$ fm), but for smaller radii the error bands exhibit a large uncertainty. Nevertheless the imaginary potentials obtained in the calculations with real double-folding potentials are in the vicinity of the best fit potentials of the MIA.

The 104 MeV data for α-^{208}Pb scattering [65] have already been analyzed by a MIA by Friedman *et al.* [67] and by Ermer *et al.* [73]. In both calculations Fourier-Bessel series were used. We performed an analysis using Laguerre polynomials. The results are shown in Fig. 6 for the differential cross section (dashed line) and in Fig. 1 for the radial behavior of the MIA potential compared with the result of the MIA analysis of Ermer *et al.* [73] and with the DF potential used in our analysis. Again it can be stated that the experimental data can be fitted as well by the DF potential as by the potential resulting from the MIA. In Fig. 1 one can see that the potentials exhibit the same behavior as the α-^{90}Zr potentials: for radii >5 fm the potential is well determined by the scattering data while for smaller radii the error band is larger. The DF potential lies well within the 1σ error band of the Laguerre potential, while the FB potential shows a deviation around 4 fm, but the volume integrals agree within the calculated errors.

IV. BOUND AND QUASIBOUND STATES, $B(E2)$ VALUES

As a second step we use the double-folded α-nucleus potential as a suitable cluster-core potential and calculate bound

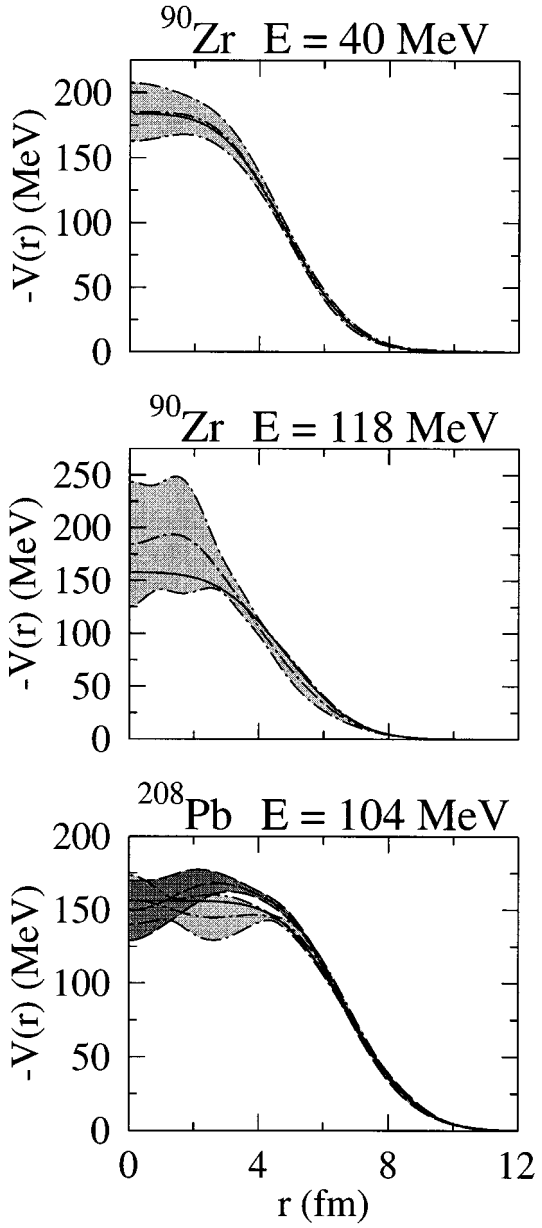

FIG. 7. Comparison of the real potentials for the elastic α scattering on ^{90}Zr at 40 and 118 MeV and on ^{208}Pb at 104 MeV. For ^{90}Zr the DF potential is shown (solid line) together with the best-fit potential of the MIA (dash-dotted line) and the error band (shaded). For Pb the DF potential (solid line), the result of the MIA using Laguerre polynomials (dash-dotted line with error band light shaded), and the result of Ermer *et al.* [73] using Fourier-Bessel series (dashed line, dark shaded) is shown.

and quasibound states properties. The wave function $u_{NL}(r)$ which describes the relative motion of the α-nucleus system is characterized by the node number N and the orbital angular momentum number L. These N and L values are related to the corresponding quantum numbers n_i and l_i of the four nucleons forming the α cluster outside the respective core:

$$Q=2N+L=\sum_{i=1}^{4}(2n_i+l_i). \tag{4.1}$$

The transition probability $B(E\mathscr{L})$ can be computed using the wave functions of the two states involved [13,74]. In the case of the clusters with Spin $S=0$ one gets

$$B(E\mathscr{L},L_i\rightarrow L_f)=\frac{e^2\beta_{\mathscr{L}}^2}{2L_i+1}\cdot\langle L_f\|Y^0_{\mathscr{L}}\|L_i\rangle^2 \cdot\left[\int_0^\infty u_{N_fL_f}(r)r^{\mathscr{L}}u_{N_iL_i}(r)dr\right]^2 \tag{4.2}$$

with

$$\beta_{\mathscr{L}}=\frac{A_T^{\mathscr{L}}Z_P+(-1)^{\mathscr{L}}A_P^{\mathscr{L}}Z_T}{(A_T+A_P)^{\mathscr{L}}}. \tag{4.3}$$

The integral in Eq. (4.2) can be solved easily if the states considered are bound states ($E<0$); in the case of quasibound states ($E>0$) the wave functions are normalized in a spherical box with a cutoff radius $R_{\rm cut}=20$ fm.

For ^{44}Ti$=\alpha\otimes^{40}$Ca we expect seven α-cluster states for the ground state ($K^\pi=0^+_1$, $Q=12$) band. Furthermore, the first few members of the theoretically predicted negative parity band ($K^\pi=0^-$, $Q=13$) have been located recently [75–78]. In a first calculation we fixed the depth of the potentials so that the computed excitation energies of the states considered coincide with the experimental values. The results are listed in Table II. The potentials obtained are very close to each other and to those deduced from optical model analysis of the α + ^{40}Ca cross section data. In a second step the excitation energies of the bound and resonance states of the two rotational bands were calculated, applying for both bands the potential deduced for the band head. The resulting level schemes are shown in Fig. 8 together with the experimental values and the results of a microscopic calculation [79]. In contrast to ^{20}Ne [13] a rotational energy spacing between the levels in ^{44}Ti is found only for the low spin states. The high spin states 8^+, 10^+, and 12^+ are tightly compressed. Therefore the agreement between the experimental and the calculated level scheme is not satisfying. Recently, Buck *et al.* [14] have shown that a better agreement can be obtained in the frame of a cluster model by using a phenomological potential with a specific geometric shape.

For the calculation of the $B(E2)$ values potentials which reproduce the experimental level scheme have been used. The resulting $B(E2)$ values are listed in Table III together with the experimental data, values resulting from shell model calculations, and values obtained in the potential model of Michel *et al.* [75]. The general agreement between experiment and this work is satisfying except the two transitions $4^+\rightarrow 2^+$ and $10^+\rightarrow 8^+$, indicating possible difficulties with the simple model ^{44}Ti $=\alpha\otimes^{40}$Ca.

$B(E\mathscr{L})$ values of ^{94}Mo $=\alpha\otimes$ ^{90}Zr have been calculated by Ohkubo [69] using the same model as in this work. Of course, we agree with the numerical results of Ohkubo, but to obtain a good agreement with the experimental data one has to introduce an effective charge of $\delta e=0.2e$. The same discrepancy between experimental and calculated $B(E\mathscr{L})$ values of ^{94}Mo has been found by Buck *et al.* [14] using a potential with a special shape which has almost the same volume integral as the folding potential of Ohkubo.

TABLE II. Energy eigenvalues, quantum numbers, and integral potential parameters of α-^{40}Ca states in ^{44}Ti.

$E_{\text{c.m.}}$(MeV) [a]	K^π	J^π	L_α	Q	λ_R	J_R (MeVfm^3)
−5.120	0_1^+	0^+	0	12	1.233	351.3
−4.036		2^+	2		1.220	347.6
−2.666		4^+	4		1.212	345.3
−1.105		6^+	6		1.211	344.9
1.388		8^+	8		1.204	343.0
2.551		10^+	10		1.236	351.9
2.919		12^+	12		1.276	363.3
1.100	0^-	1^-	1	13	1.245	354.6
2.220		3^-	3		1.236	352.1
4.310		5^-	5		1.220	347.4

[a]Energies are given relative to the α separation energy in ^{44}Ti [77].

$B(E\mathscr{L})$ values for the nucleus ^{212}Po = $\alpha \otimes$ ^{208}Pb have been calculated by Buck *et al.* [14] using again the special shaped Saxon-Woods potential and a wave function with $Q=18$ or $Q=20$. But it has been shown that the properties of ^{212}Po can be described as well using our folding potential model using a $Q=22$ wave function [74,69].

V. THE ENERGY AND MASS DEPENDENCE

The energy dependence for the volume integrals of both the real and the imaginary part of the potential is plotted in Figs. 9 and 10. The integral potential values clearly indicate a systematic energy and mass dependence.

For all nuclei considered the volume integrals of the imaginary part of the potential can be described by a *BR* parametrization (2.12). The parameters are listed in Table IV. For the double magic nuclei ^{16}O and ^{40}Ca similar values are found: the saturation value is around J_0 = (118 ± 6) MeV fm^3, the ''width'' of the rise in the BR parametrization is Δ = (30 ± 5) MeV. The values found in the α-^{208}Pb system are slightly smaller: J_0 = 77 MeV fm^3 and Δ = 24 MeV. For the other nuclei (^{58,60}Ni, ^{90}Zr, and the $N=82$ isotopes) the values for Δ are considerably smaller, giving a faster rise of the depth of the volume integral J_I. This is an indication of the large number of open channels at relatively small energies. The saturation value J_0, which is reached at energies above $E_{\text{c.m.}} > 100$ MeV, is decreasing with increasing mass for all nuclei considered. This has already been stated by Friedman *et al.* [67], Shridhar *et al.* [80], and Nolte

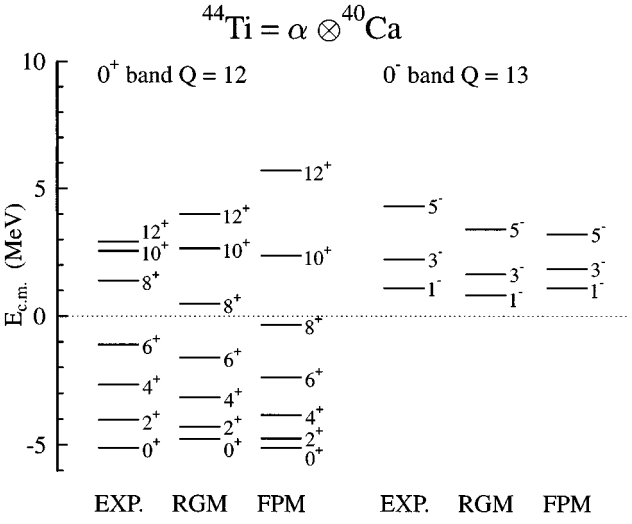

FIG. 8. Experimental level scheme for the $Q=12$ and $Q=13$ rotational band in ^{44}Ti together with the results of RGM [79] and our folding-potential model (FPM) calculation.

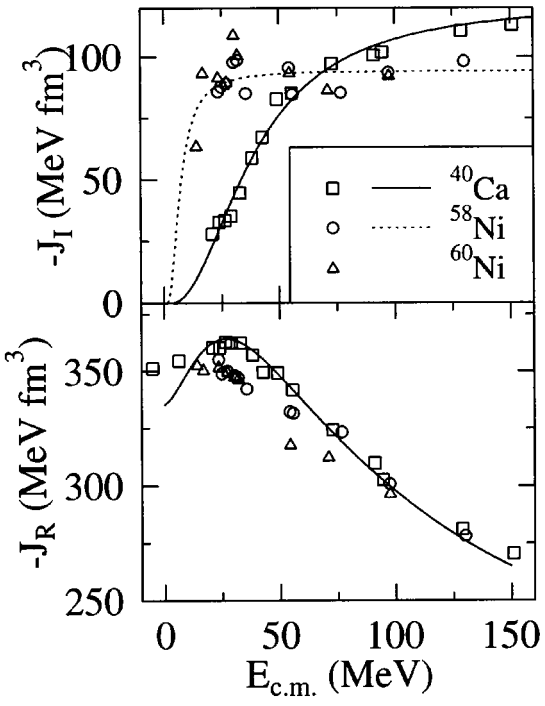

FIG. 9. Volume integrals of the nuclear potentials derived from the analysis of the elastic α-scattering data on ^{40}Ca and ^{58,60}Ni. In the upper part the volume integrals of the imaginary part together with BR parametrizations of the energy dependence are shown. In the lower part volume integrals of the real part of the potentials are shown. The solid line is the result of a dispersion analysis for α-^{40}Ca.

TABLE III. $B(E2)$ values in α-^{40}Ca (all values in $e^2\text{fm}^4$).

	Experiment	Ref. [75]	Refs. [82,83]	This work
$2^+\rightarrow 0^+$	120 ± 30	107.3	40.0	109.0
$4^+\rightarrow 2^+$	280 ± 60	146.4	53.4	148.5
$6^+\rightarrow 4^+$	160 ± 20	140.2	51.6	141.8
$8^+\rightarrow 6^+$	>14	118.1	44.0	119.1
$10^+\rightarrow 8^+$	140 ± 30	74.9	32.0	73.6
$12^+\rightarrow 10^+$	40 ± 8	33.6	17.3	33.7

et al. [10]. The saturation values given in these references are in agreement with our results.

The energy dependence of the real part of the potential shows a characteristic behavior for all nuclei considered. Starting from the values that result from the analyses of the bound and quasibound states J_R is increasing with increasing energy until a maximum is reached at around $E_{\text{c.m.}} \approx 25$ MeV. For energies above the maximum J_R is decreasing again. This behavior has already been observed in the analyses of the α-^{40}Ca scattering by Gubler *et al.* [6] and in the α-^{16}O scattering [17]. Nolte *et al.* [10] give a global potential in which strength is decreasing with increasing energy with a slope around -0.6 MeV fm^3/MeV for energies $E_\alpha >$ 80 MeV.

The decrease of the volume integral J_R with increasing energy is approximately linear in the energy range between $E_{\text{c.m.}} \approx 25$ and $E_{\text{c.m.}} \approx 120$ MeV with a slope of ≈ -1 MeV fm^3/MeV in the case of ^{40}Ca and ≈ -0.5 MeV fm^3/MeV for all nuclei with $A> 90$. For the two Ni isotopes analyzed the slope is somewhere in between. For all nuclei the slope becomes smaller for energies $E_{\text{c.m.}} > 120$ MeV. This result is in good agreement with the results of Friedman *et al.* [67] and a data compilation of England *et al.* [39] but in contradiction to the recent work of Ohkubo [69].

The volume integrals of the real part of the potential J_R exhibit a strong mass dependence: the values for the α-^{40}Ca system are significantly smaller than those for the α-^{16}O system [17]. For nuclei with masses $A\geqslant 90$ the strength of the real part of the potential becomes independent of the target mass (see Fig. 10). In the range of the maximum at $E_{\text{c.m.}}\approx 25$ MeV one finds values for J_R around $330-335$ MeV fm^3 which are about 25 MeV fm^3 below those for ^{40}Ca. In this energy range the volume integrals for the Ni isotopes lie between those of ^{40}Ca and ^{90}Zr/^{208}Pb, whereas at higher energies $E_{\text{c.m.}}\geqslant 50$ MeV they coincide with the values of the heavier target nuclei. Volume integrals for very low energies have been calculated by adjusting the strength parameter λ of the folding potential to bound state energies (see Sec. IV).

This observed mass dependence is in agreement with that given by England *et al.* [39] for $E_\alpha = 25$ MeV and target nuclei with $50 \leqslant A \leqslant 93$ and that of Friedman [67] for $E_\alpha = 104$ and 140 MeV and target nuclei with $40 \leqslant A \leqslant 208$.

For the calculation of the subtracted dispersion relation [Eq. (2.11)] assumptions about the energy behavior of the volume integral J_I for the imaginary part of the potentials at higher energies are necessary. In the calculations presented here we used the parametrization (2.12) up to an energy $E = 220$ MeV whereas for higher energies up to $E_L = 10^{20}$ MeV a linear decrease of J_I was assumed with $J_I(E_L) = 0$

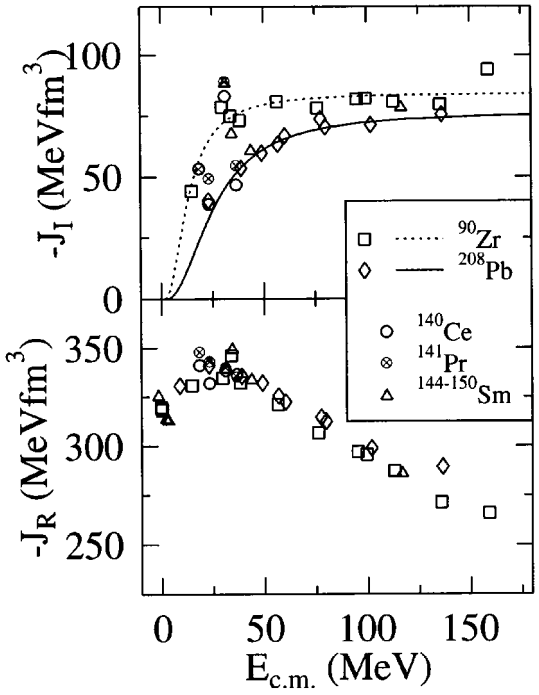

FIG. 10. Same as Fig. 9, but for elastic α scattering on ^{90}Zr, target nuclei with $N = 82$, and ^{208}Pb.

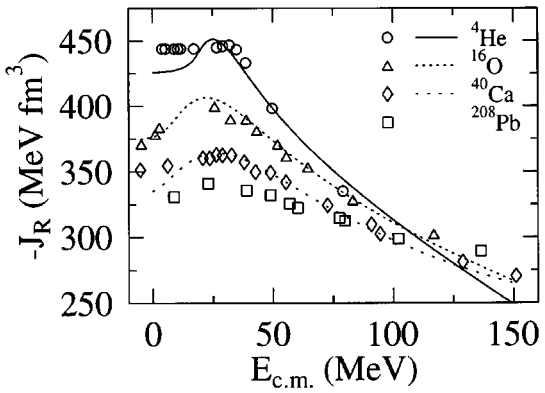

FIG. 11. Same as Fig. 9, but for elastic α scattering on ^{4}He [81], ^{16}O [17], ^{40}Ca, and ^{208}Pb. The data points are derived from OM analyses using double-folded potentials; the lines are the result of a dispersion analysis.

TABLE IV. BR parametrizations for the energy dependence of the imaginary volume integral J_I.

Target nucleus	E_0 MeV	J_0 MeV fm^3	Δ MeV
^{16}O [a]	6.05	114.4	25.8
^{40}Ca	3.35	122.2	36.3
^{58}Ni	1.45	99.0	17.8
^{90}Zr	1.78	84.3	11.8
^{208}Pb	2.62	76.6	23.8

[a]The data for ^{16}O are taken from Ref. [17].

[17]. In this the integral (2.11) can be evaluated directly.

In Fig. 11 the volume integrals for the real part of the potential resulting from the OM calculations are shown for the systems α-^{4}He [81], α-^{16}O [17], α-^{40}Ca, and α-^{208}Pb together with theoretical curves which represent the mass and energy dependence of the volume integral of the real part of the potential. The real potential in these calculations is the sum of the channel potential derived from the double-folding procedure and normalized to the reference energy $E_S = 61$ MeV, and the calculated dispersive part.

For the systems α-^{4}He, α-^{16}O, and α-^{40}Ca the observed energy dependence can be well described by the interplay of the energy dependence of the folding potential and the dispersive corrections. But this procedure fails to reproduce the energy dependence of the volume integral of the real part of the nuclear potential J_R for the α-^{208}Pb system. The double-folding calculation for the channel potential gives a linear decrease of J_R with the energy. In the case of the α-^{208}Pb the slope is about -0.4 MeV fm^3/MeV. After adding the result of the dispersion relation a much stronger energy dependence is obtained as it results from the analysis of the experimental data. In order to describe the observed experimental energy dependence one would have to alter the slope of the energy dependence of the channel potential from -0.4 MeV fm^3/MeV to -0.1 MeV fm^3.

For the other α-nucleus systems studied, the linear decrease of the volume integral J_R as obtained by the OM analysis coincides with that from the channel potential derived from the double-folding procedure. In addition the steep rise of the strength of the imaginary potential at low energies results in a larger amplitude of the dispersive correction and in an energy dependence much too strong in comparison with the results of the OM analysis of the experimental data. This means that the discrepancy observed in the α-^{208}Pb sytem is even higher for the nonmagic nuclei analyzed in this work. This result is indicating that the DDM3Y NNI is reaching the limit of a suitable application if one is considering dispersive corrections additionally.

VI. CONCLUSION

Differential cross sections for the elastic scattering of α particles on ^{40}Ca, ^{58,60}Ni, ^{90}Zr, ^{140}Ce, ^{141}Pr, ^{144}Sm, and ^{208}Pb have been analyzed in the optical model in a wide range of energies. The real part of the potential was deduced by a double-folding procedure using a density dependent effective nucleon-nucleon interaction. One energy dependent parameter is needed to adjust the strength of the potential. For the imaginary part different parametrizations such as i.e., Woods-Saxon functions or Fourier-Bessel series are employed. The elastic scattering cross sections are described very satisfactorily for incident energies between about 25 and 150 MeV, for some target nuclei even up to 340 MeV.

Bound and quasibound state properties of ^{44}Ti have been calculated in this work using the same folding potential as in the OM calculations. The properties of ^{8}Be, ^{20}Ne, ^{94}Mo, and ^{212}Po have been analyzed successfully in this model in several previous papers.

Some model independent analyses applying Laguerre series for the potentials have been performed. The differences in the description of the experimental differential cross sections using either double-folded or model independent potentials are small, and the double-folded potentials lie within the error bars of the model independent potential. Consequently, the shape of the folding potential is well suited for the description of elastic α scattering.

The volume integrals of the real potential show a systematic behavior over the whole analyzed mass and energy range. Applying the subtracted dispersion relation in combination with the DDM3Y interaction used in the calculation of the double-folded channel potential, the observed energy dependence of the volume integral of the real part of the potential can be reproduced satisfactorily only for the systems α-^{4}He, α-^{16}O, and α-^{40}Ca. For heavier systems, the observed energy dependence is weaker than expected from the dispersion relation.

In conclusion, we are able to reproduce as well angular distributions of elastic scattering as bound state properties using double-folded potentials with the DDM3Y interaction in a wide range of masses and energies. Furthermore, from the systematic behavior of the volume integrals it is possible to predict a realistic strength of the real and imaginary part of the α-nucleus potential for systems that cannot be analyzed directly using scattering experiments. The importance of the so-called ''family problem'' is significantly reduced by this work.

ACKNOWLEDGMENTS

We would like to thank Prof. H. Clement and Prof. H. J.

Gils for fruitful discussions, and Dr. G. Bartnitzky for supplying various computer codes. Financial support of the Deutsche Forschungsgemeinschaft under contract Sta290 and Mu705 is gratefully acknowledged. We are thankful to Prof. B. Bonin, Prof. L. W. Put, and Prof. C. A. Wiedner for giving us their original data.

[1] H. Oberhummer and G. Staudt, in *Nuclei in the Cosmos*, edited by H. Oberhummer (Springer Heidelberg, 1991), p. 29.
[2] P. Mohr, H. Abele, R. Zwiebel, G. Staudt, H. Krauss, H. Oberhummer, A. Denker, J. W. Hammer, and G. Wolf, Phys. Rev. C **48**, 1420 (1993).
[3] P. Mohr, V. Kölle, S. Wilmes, U. Atzrott, G. Staudt, J. W. Hammer, H. Krauss, and H. Oberhummer, Phys. Rev. C **50**, 1543 (1994).
[4] P. Mohr, H. Abele, V. Kölle, G. Staudt, H. Oberhummer, and H. Krauss, Z. Phys. A **349**, 339 (1994).
[5] F. Michel and R. Wanderpoorten, Phys. Rev C **16**, 142 (1977).
[6] H. P. Gubler, U. Kiebele, H. O. Mayer, G. R. Plattner, and I. Sick, Nucl. Phys. **A351**, 29 (1981).
[7] L. W. Put and A. M. J. Paans, Nucl. Phys. **A291**, 93 (1977).
[8] E. Friedman and C. J. Batty, Phys. Rev. C **17**, 34 (1978).
[9] H. J. Gils, E. Friedman, H. Rebel, J. Buschmann, S. Zagromski, H. Klewe-Nebenius, B. Neumann, R. Pesl, and G. Bechtold, Phys. Rev. C **21**, 1239 (1980).
[10] M. Nolte, H. Machner, and J. Bojowald, Phys. Rev. C **36**, 1312 (1987).
[11] V. Avrigeanu, P. E. Hodgson, and M. Avrigeanu, Phys. Rev. C **49**, 2136 (1994).
[12] B. Buck, C. B. Dover, and J. P. Vary, Phys. Rev. C **11**, 1803 (1975).
[13] B. Buck and A. A. Pilt, Nucl. Phys. **A280**, 133 (1977).
[14] B. Buck, A. C. Merchant, and S. M. Perez, Phys. Rev. C **51**, 559 (1995).
[15] B. Buck, J. C. Johnston, A. C. Merchant, and S. M. Perez, Phys. Rev. C **52**, 1840 (1995).
[16] B. Buck *et al.*, Phys. Rev. C, submitted.
[17] H. Abele and G. Staudt, Phys. Rev C **47**, 742 (1993).
[18] A. M. Kobos, B. A. Brown, R. Lindsay, and R. Satchler, Nucl. Phys. **A425**, 205 (1984).
[19] J. Fritze, R. Neu, H. Abele, F. Hoyler, G. Staudt, P. D. Eversheim, F. Hinterberger, and H. Müther, Phys. Rev. C **43**, 2307 (1991).
[20] K. Kocher, R. Neu, F. Hoyler, H. Abele, P. Mohr, G. Staudt, P. D. Eversheim, and F. Hinterberger, Phys. Rev. C **45**, 123 (1992).
[21] H. de Vries, C. W. de Jager, and C. de Vries, At. Data Nucl. Data Tables **36**, 495 (1987).
[22] J.-P. Jeukenne, A. Leujenne, and C. Mahaux, Phys. Rev. C **16**, 80 (1977).
[23] J.-P. Jeukenne and C. Mahaux, Z. Phys. A **302**, 233 (1981).
[24] T. Rohwer, computer code WWFIT, University of Tübingen, unpublished.
[25] F. Petrovich, R. J. Philpott, A. W. Carpenter, and J. A. Carr, Nucl. Phys. **A425**, 609 (1984).
[26] C. J. Horowitz and B. D. Serot, Nucl. Phys. **A368**, 503 (1981).
[27] C. Mahaux, H. Ngo, and G. R. Satchler, Nucl. Phys. **A449**, 354 (1986); **A456**, 134 (1986).
[28] J. C. Pacheco, J. L. Ferrero, N. Vinh Mau, and B. Bilwes, Phys. Lett. B **267**, 455 (1991).
[29] G. Pantis, H. Fiedeldey, and S. A. Sofianos, J. Phys. G **21**, 1079 (1995).
[30] G. E. Brown and M. Rho, Nucl. Phys. **A372**, 397 (1981).
[31] H. G. Andresen and H. Müller, in *Advanced Methods in the Evaluation of Nuclear Scattering Data*, *Proceedings*, edited by H. J. Krappe and R. Lipperheide, Lecture Notes in Physics Vol. 236 (Springer-Verlag Berlin, 1985).
[32] H. Clement, G. Bartnizky, H. Abele, M. Ermer, H. G. Bohlen, B. Gebauer, Th. Kirchner, Ch. Langner, M. von Lucke-Petsch, W. von Oertzen, A. Ostrowski, M. Wilpert, Th. Wilpert, A. S. Demyanova, A. A. Ogloblin, S. A. Goncharov. and F. A. Gareev, in *Proceedings of the Conference of Nuclear Structure and Nuclear Reactions at Low and Intermediate Energies*, Dubna, 1992 (JINR, Dubna, 1993).
[33] M. Ermer, Ph.D. thesis, University of Tübingen, 1991.
[34] H. Abele, computer code GOMPF, University of Tübingen, unpublished.
[35] J. Raynal, computer code ECIS79, CEN Saclay, unpublished.
[36] H. P. Gubler, U. Kiebele, H. O. Meyer, G. R. Plattner, and I. Sick, Nucl. Phys. **A351**, 29 (1981).
[37] Th. Delbar, Gh. Gregoire, G. Paic, R. Ceuleneer, F. Michel, R. Vanderporten, A. Budzanowski, H. Dabrowski, L. Freindl, K. Grotowski, S. Micek, R. Planeta, A. Strzalkowski, and K. A. Eberhard, Phys. Rev. C **18**, 1237 (1978).
[38] Z. Maijka, H. Gils, and H. Rebel, Z. Phys. A **288**, 139 (1978).
[39] J. B. A. England, S. Baird, D. H. Newton, T. Picazo, E. C. Pollacco, G. J. Pyle, P. M. Rolph, J. Alabau, E. Casal, and A. Garcia, Nucl. Phys. **A388**, 573 (1982).
[40] A. Budzanowski, H. Dabrowski, L. Freindl, K. Grotowski, S. Micek, R. Planeta, A. Strzalkowski, M. Bosman, P. Leleux, P. Macq, J. P. Meulders, and C. Pirart, Phys. Rev. C **17**, 951 (1978).
[41] D. G. Madland, P. Schwandt, W. T. Sloan, P. Shapiro, and P. P. Singh, Phys. Rev. C **9**, 1002 (1974).
[42] H. H. Chang, B. W. Ridley, T. H. Braid, T. W. Conlon, E. F. Gibson, and N. S. P. King, Nucl. Phys. **A270**, 413 (1976).
[43] H. Rebel, R. Löhken, G. W. Schweimer, G. Schatz, and G. Hauser, Z. Phys. A **256**, 258 (1972).
[44] M. Lassaut, Nucl. Phys. **A442**, 1 (1985).
[45] J. Albinski, A. Budzanowski, H. Dabrowski, Z. Rogalska, S. Wiktor, H. Rebel, D. K. Srivastava, C. Alderliesten, J. Bojowald, W. Oelert, C. Mayer-Böricke, and P. Turek, Nucl. Phys. **A445**, 477 (1985).
[46] W. D. Ploughe, J. W. Kerns, W. W. Jacobs, and P. Schwandt, Indiana Cyclrotron Facility Report 1980, 78.
[47] B. Bonin, N. Alamanos, B. Berthier, G. Bruge, H. Faraggi, J. C. Lugol, W. Mittig, L. Papineau, A. I. Yavin, J. Arvieux, L. Farvacque, M. Buenerd, and W. Bauhoff, Nucl. Phys. **A445**, 381 (1985).
[48] T. B. Robinson and V. R. W. Edwards, Nucl. Phys. **A301**, 36 (1978)

[49] B. D. Watson, D. Robson, D. D. Tolbert, and R. H. Davis, Phys. Rev. C **4**, 2240 (1971).
[50] P. Mailandt, J. S. Lilley, and G. W. Greenless, Phys. Rev. C **8**, 2189 (1973)
[51] E. J. Martens and A. M. Bernstein, Nucl. Phys. **A117**, 241 (1968).
[52] D. Rychel, R. Gyufko, B. van Krüchten, M. Lahanas, P. Singh, and C. A. Wiedner, Z. Phys. A **326**, 455 (1987).
[53] V. Corcialciuc, H. J. Gils, H. Rebel, J. Buschmann, R. Pesl, R. Dumitrescu, S. Zagromski, and K. Feißt, Z. Phys. A **305**, 351 (1982)
[54] D. A. Goldberg, S. M. Smith, and G. F. Burdzik, Phys. Rev. C **10**, 1362 (1974).
[55] I. Brissaud, Y. le Bornec, B. Tatischeff, L. Bimbot, M. K. Brussel, and G. Duhamel, Nucl. Phys. **A191**, 145 (1972).
[56] P. Guazzoni and L. Zetta, University of Milano, private communication.
[57] H. W. Baer, H. C. Griffin, and W. S. Gray, Phys. Rev. C **3**, 1398 (1971).
[58] T. Ichihara, H. Sakaguchi, M. Nakamura, T. Noro, H. Sakamoto, H. Ogawa, M. Yosoi, M. Ieiri, N. Isshiki, Y. Takeuchi, and S. Kobayashi, Phys. Rev. C **35**, 931 (1987).
[59] J. S. Lilley, M. A. Francy, and Da Hsuan Feng, Nucl. Phys. **A342**, 165 (1980).
[60] A. M. Baxter, S. Hinds, R. H. Spear, T. H. Zabel, and R. Smith, Nucl. Phys. **A369**, 25 (1981).
[61] U. Atzrott, Ph.D. thesis, University of Tübingen, 1995.
[62] P. David, J. Debrus, H. Essen, F. Lübke, H. Mommsen, R. Schoenmackers, W. Soyez, H. V. v. Geramb, and E. F. Hefter, Z. Phys. A **278**, 281 (1976).
[63] R. Tickle and W. S. Gray, Nucl. Phys. **A247**, 187 (1975).
[64] R. Perry, A. Nadasen, D. L. Hendrie, P. G. Roos, and N. S. Chant, Phys. Rev. C **24**, 1471 (1981).
[65] V. Corcialciuc, H. Rebel, R. Pesl, and H. J. Gils, J. Phys. G **9**, 177 (1983).
[66] D. A. Goldberg, S. M. Smith, H. G. Pugh, P. G. Roos, and N. S. Wall, Phys. Rev. C **7**, 1938 (1973).
[67] E. Friedman, H. J. Gils, H. Rebel, and R. Pesl, Nucl. Phys. **A363**, 137 (1981).
[68] Dao Tien Khoa and O. M. Knyazkov, Z. Phys. A **328**, 67 (1987).
[69] S. Ohkubo, Phys. Rev. Lett. **74**, 2176 (1995).
[70] R. Neu and F. Hoyler, Phys. Rev. C **46**, 208 (1992).
[71] J. Raynal, Computerprogramm ECIS90, CEN Saclay, unpublished, modified by G. Bartnitzky, University of Tübingen.
[72] G. Bartnitzky, Programm READECIS, University of Tübingen, unpublished.
[73] M. Ermer, H. Clement, G. Frank, P. Grabmayr, N. Heberle, and G. J. Wagner, Phys. Lett. B **224**, 40 (1989).
[74] F. Hoyler, P. Mohr, and G. Staudt, Phys. Rev. C **50**, 2631 (1994).
[75] F. Michel, G. Reidemeister, and S. Ohkubo, Phys. Rev. C **37**, 292 (1988).
[76] S. Ohkubo, Phys. Rev. C **38**, 2377 (1988).
[77] T. Yamaya, S. Oh-ami, M. Fujiwara, T. Itahashi, K. Katori, M. Tosaki, S. Kato, S. Hatori, and S. Ohkubo, Phys. Rev. C **42**, 1935 (1990).
[78] P. Guazzoni, M. Jaskola, L. Zetta, C.-Y. Kim, T. Udagawa, and G. Bohlen, Nucl. Phys. **A564**, 425 (1993).
[79] T. Wada and H. Horiuchi, Phys, Rev. C **38**, 2063 (1988).
[80] A. Shridhar, N. Lingappa, S. K. Gupta, and S. Kailas, Phys. Rev. C **30**, 1760 (1984).
[81] H. Abele, Ph.D. thesis, University of Tübingen, 1992.
[82] T. Motoba and K. Itonaga, Suppl. Prog. Theor. Phys. **65**, 136 (1979).
[83] K. Itonaga, Prog. Theor. Phys. **66**, 2103 (1981).